Monthly Notices of the ROYAL ASTRONOMICAL SOCIETY

MNRAS **525,** 3486–3498 (2023) https://doi.org/10.1093/mnras/stad2510
Advance Access publication 2023 August 21

Photometric metallicities of fundamental-mode RR Lyr stars from Gaia *G* band photometry of globular-cluster variables

Johanna Jurcsik[1]★ and Gergely Hajdu[2]

[1]*Konkoly Observatory, Research Centre for Astronomy and Earth Sciences, ELKH, Konkoly Thege Miklós út 15-17 , 1121 Budapest, Hungary*
[2]*Nicolaus Copernicus Astronomical Centre, Polish Academy of Sciences, Bartycka 18, PL-00-716 Warsaw, Poland*

Accepted 2023 August 16. Received 2023 July 6; in original form 2023 May 17

ABSTRACT

Photometric metallicity formulae of fundamental-mode RR Lyr (RRab) stars are presented using globular-cluster data exclusively. The aim is to check whether this selection may help increasing the overall accuracy of the fits and eliminating the systematic bias of the photometric results, namely that they tend to overestimate [Fe/H] of the most metal-poor variables. The *G* band time-series data available in the Gaia DR3 archive and a new compilation of the published spectroscopic globular cluster [Fe/H] values on a uniform solar reference metallicity scale are utilized. We have derived a new $[Fe/H]_{phot} - P, \varphi_{31}$ formula, and have diagnosed that no significant increase in the accuracy of the fit can be achieved using non-linear or multiparameter formulae. The best result is obtained when different formulae are applied for variables with Oosterhoff (Oo)-type I and II properties. However, even this solution cannot eliminate the systematic bias of the results completely. This separation of the variables has also led to the conclusion that the photometric estimates of the [Fe/H] are less reliable for the Oo-type II variables than for the Oo-type I sample. Published $[Fe/H]_{phot}$ values and the results of the available photometric formulae in the Gaia *G* band are compared with the present results. It is found that each of the solutions yields very similar results, with similar accuracy and systematic biases. Major differences are detected only in the zero-points of the [Fe/H] scales, and these offsets are larger than differences in the accepted solar reference values would explain.

Key words: techniques: photometric – stars: abundances – stars: variables: RR Lyrae – globular clusters: general.

1 INTRODUCTION

RRab stars, the fundamental-mode radial pulsators on the horizontal branch in the evolutionary stage of core helium burning, are of great astrophysical importance because their physical properties can be easily estimated from the properties of their light variation. The Bailey diagram, which traces the variation of the luminosity amplitude of RR Lyrae (RRL) stars as a function of the pulsation period, is a fundamental diagnostic for studying RRL stars (as a recent interpretation of the Bailey diagram read Bono et al. 2020). Several relations between the physical properties and the light curve (LC) parameters of RRL stars has been established based on theoretical and empirical studies. These relations are widely employed in the study of individual variables, as well as their host stellar populations (see e.g. Bellinger et al. 2020).

The luminosity and the radius of RRL stars correlate with the pulsation period, which can be measured with the highest accuracy out of all physical parameters, and the metallicity (see e.g. Marconi et al. 2015; Mullen et al. 2023). The knowledge of the metallicity of stars is crucial for evolutionary and cosmological aspects, too. Therefore, this is not surprising that several metallicity formulae in different photometric bands has been published after the invention of a very simple, linear $[Fe/H]-P, \varphi_{31}$ relation by Jurcsik & Kovács (1996). The accuracy of these photometric metallicities are estimated to be about 0.13−0.16 dex, typically. The photometric [Fe/H] formulae are widely used to determine globular cluster (GC) metallicities (see e.g. Arellano Ferro 2022), although these formulae systematically overestimate the metallicity of the most metal-poor clusters by ∼0.2 dex.

The accuracy of an empirical relation between different observables depends on the accuracy of the input data that the calibration of the formula is based on, and also on the limits of the inherent physical connection between the compared quantities. The estimate of systematic and random errors of the observations can be considered reliable in most of the cases, however, the inherent limits of empirical relations is usually unknown.

Concerning the calibration of the photometric metallicity, the most problematic issue is the accepted [Fe/H] values of stars in the calibrating sample. The scatter of the different spectroscopic [Fe/H] data of the calibrating stars that are used to establish a photometric metallicity formulae is about 0.15 dex, typically. Therefore, this may account for the similar final accuracy of the predictions. However, what the best possible attainable accuracy is, is an open question for any photometric [Fe/H] formula.

Regarding field stars, several high-dispersion spectroscopic studies of individual stars and large spectroscopic survey data have been published, but because of the problems with the dynamic atmosphere of RRL stars, the atmospheric parameter determinations, the line list adopted and several other factors, the iron abundance estimates are very divergent in some cases.

★ E-mail: jurcsik.johanna@gmail.com

On the other hand, the GC metallicities seem to have reached a consensus. These [Fe/H] values are determined using high-resolution spectra of giant stars for most of the clusters, and have smaller dispersion for the individual clusters than the [Fe/H] observations of individual field RR Lyrae stars, typically.

Therefore, in this paper, we make an attempt to establish new photometric metallicity formulae using GC data exclusively, to see whether this would help to improve the overall fitting accuracy and to reduce the systematic bias towards the metal-poor end of the [Fe/H] scale of the predictions. For this purpose we utilize the time-series photometry from Gaia DR3, which, as of today, yields the most homogeneous, complete sample of good quality LCs of GC variables.

2 THE DATA

2.1 Target selection

According to our present day knowledge, most of the GCs host multiple generations of stars of different chemical compositions. Several studies of the *Hubble Space Telescope* UV Legacy Survey of Galactic globular clusters (Milone et al. 2015), which utilizes the pseudo-two-colour diagrams (chromosome maps), indicate that the elemental distributions of the different stellar populations in GCs are divergent. High-resolution spectroscopic (HRS) studies of individual clusters are in line with this picture.

Spread in the iron content has been also revealed in a few clusters, but its range typically does not exceed 0.1−0.2 dex and/or the population of the extreme metallicity stars is marginal in most cases (see e.g. table 8 in Marino et al. 2021). Moreover, some of the results concerning cluster metallicities are controversial, e.g. Carretta et al. (2010) concluded that NGC 6715 (M54) in the Sagittarius dwarf galaxy is similar to ω Cen in its [Fe/H] range and dispersion, but according to the recent analyses of the APOGEE spectra its [Fe/H] spread is found to be smaller (Mészáros et al. 2020; Fernández-Trincado et al. 2021). Mucciarelli & Cosmic-Lab Team (2016) have shown that even the chemical composition analyses of HRS observations may lead to spurious results concerning the metallicity spread in some cases.

Therefore, we decided to utilize every cluster with at least a single RRab star that have Gaia *G* band LC in the process of deriving connection between the cluster metallicity and the LC parameters of RRab stars.

The only exceptions are: i) the most complex Galactic GC, ω Cen, ii) the three Oosterhoff-type III (OoIII) GCs (NGC 6304, NGC 6388, and NGC 6441), and iii) NGC 104 (47 Tuc). The long-period and metal-rich variables in the OoIII clusters and in 47 Tuc do not yield reliable photometric metallicity values. The results on the photometric metallicities of these clusters are discussed in Section 4.2.

The catalogue of the intrinsic iron-abundance spread of GCs (Bailin 2019) lists three clusters with iron dispersion significantly larger than 0.1 dex, namely NGC 6273, NGC 6715, and ω Cen. However, the photometric metallicity of the RRab stars in NGC 6273 and NGC 6715 are in good agreement with the mean cluster metallicity values, without showing larger dispersion than in other clusters, therefore these stars are kept in the calibrating sample of the metallicity formula.

2.2 Spectroscopic data

Since the 2010 electronic edition of the catalogue of GC data (Harris 1996, 2010, hereafter H10) several spectroscopic surveys and detailed chemical composition analyses of stars in GCs have been published. The latest compilation of GC metallicities by B. Dias (Dias et al. 2015, 2016a, b; Vásquez et al. 2018) does not include all the published HRS data of individual GCs. Therefore, to obtain the possible best result, we have collected all the HRS [Fe/H] measurements, which were not included in the H10 catalogue, of the GCs of our interest. As HRS observations are not available for some GCs, the Ca II triplet metallicity values published by Saviane et al. (2012); Dias et al. (2016b); Vásquez et al. (2018), and Geisler et al. (2023) are also taken into account.

The [Fe/H] values published by different authors refer to different solar compositions. For example the Gaia-ESO Survey (Pancino et al. 2017) accepts $\log\epsilon\mathrm{Fe}_\odot = 7.45$ (Grevesse, Asplund & Sauval 2007) solar value, while the H10 [Fe/H] values are matched to the UVES scale (Carretta et al. 2009) adopting $\log\epsilon\mathrm{Fe}_\odot = 7.54$ (Gratton et al. 2003).

Most of the published [Fe/H] values of RRL stars are matched to the $\log\epsilon\mathrm{Fe}_\odot = 7.50$ (Asplund et al. 2009) value, therefore, in order to obtain the possible most homogeneous GC metallicities all the data used are transposed to this value. This decision results in a +0.04 dex offset of the H10 data. The results published by Mészáros et al. (2020) and Masseron et al. (2019) are 0.064 dex less metal-poor than the cluster [Fe/H] values of Carretta et al. (2009) and Pancino et al. (2017), even when using the same solar reference value (see fig. 4 in Mészáros et al. 2020), therefore these data are also corrected for this systematic difference. The Ca II triplet results are also matched to the accepted scale applying 0.02 and 0.04 dex corrections on the Dias et al. (2016b), Vásquez et al. (2018), Geisler et al. (2023), and Saviane et al. (2012) data, respectively.

There are several other reasons of systematic differences between the spectroscopic [Fe/H] results. Differences in the model atmospheres, the ionization state of the lines used, the treatment of non-local thermodynamic equilibrium (LTE) effects, etc., each may lead to systematically different results. However, to treat all these problems completely is beyond the scope of this paper.

The [Fe/H] values published by Roederer & Sneden (2011), Roederer & Thompson (2015), and Sobeck et al. (2011) for NGC 6341, NGC 4833, and NGC 7078, respectively, are about 0.3−0.4 dex more metal-poor than any other published [Fe/H] values of these clusters. Therefore, we omit these values when calculating the cluster mean [Fe/H] values. These are the only available HRS data which are not involved in the averaging.

The [Fe/H] values accepted are the weighted mean values of the H10 data, the additional HRS abundance determinations, and the low-resolution Ca II triplet equivalent-widths measurement results using weights of 3, 2, and 1, respectively. Although these weights are arbitrary, taking into account that the H10 catalogue incorporates all the measurements prior 2010, its weight of 3 is reasonable.

The accepted average [Fe/H] values of the clusters with at least one Gaia *G* band RRL LC are listed in Table 1. The H10 metallicities on the accepted solar-composition scale are also given in the table for comparison. The derived mean cluster [Fe/H] values are compared with the Carretta et al. (2009) UVES values, the H10 catalogue data, and the compilation of B. Dias (Dias et al. 2015, 2016a, b; Vásquez et al. 2018), each shifted to the same scale accepting $\log\epsilon\mathrm{Fe}_\odot = 7.50$ solar value, in Fig. 1.

Table 1. Accepted spectroscopic [Fe/H] values of GCs.

Cluster	$[Fe/H]_{mean}$	rms	$[Fe/H]^{*}_{H10}$	Reference	Cluster	$[Fe/H]_{mean}$	rms	$[Fe/H]^{*}_{H10}$	Reference
Arp2	−1.710	–	−1.71	1	NGC 6316	−0.408	0.046	−0.41	1,3,4
Djo2	−0.805	0.212	−0.61	1,2,3,4,5	NGC 6333	−1.730	–	−1.73	1
IC 4499	−1.490	–	−1.49	1	NGC 6341	−2.304	0.038	−2.27	1,9,10,70
NGC 362	−1.166	0.070	−1.22	1,6,7,8,9,10,11,12	NGC 6355	−1.383	0.053	−1.33	1,3,4,71
NGC 1261	−1.272	0.036	−1.23	1,13,14,15	NGC 6362	−1.024	0.065	−0.95	1,72,73
NGC 1851	−1.148	0.081	−1.14	1,7,8,9,10,16,17,18,19	NGC 6366	−0.580	0.052	−0.55	1,3,4,74,75
NGC 1904	−1.553	0.023	−1.56	1,7,8,9,10	NGC 6401	−1.030	0.073	−0.98	1,3,4,5
NGC 2298	−1.865	0.043	−1.88	1,21,22	NGC 6402	−1.196	0.054	−1.24	1,76
NGC 2419	−2.113	0.019	−2.11	1,23,24	NGC 6426	−2.243	0.116	−2.11	1,3,4,77
NGC 2808	−1.088	0.062	−1.10	1,3,7,8,9,10,25,26,27,28,29,30,	NGC 6453	−1.490	0.038	−1.46	1,3,4
NGC 3201	−1.464	0.063	−1.55	1,3,9,10,32,33,34,35,36	NGC 6535	−1.814	0.078	−1.75	1,78
NGC 4147	−1.792	0.039	−1.76	1,37	NGC 6541	−1.770	–	−1.77	1
NGC 4590	−2.274	0.084	−2.19	1,3,9,10,38	NGC 6558	−1.162	0.106	−1.28	1,3,25,79,80
NGC 4833	−1.899	0.073	−1.81	1,7,8,39	NGC 6569	−0.784	0.094	−0.72	1,3,25,81,82
NGC 5024	−2.026	0.035	−2.06	1,9,10,40,41,42	NGC 6584	−1.500	0.049	−1.46	1,83
NGC 5053	−2.205	0.029	−2.23	1,9,10,42,43	NGC 6626	−1.284	0.005	−1.28	1,84
NGC 5272	−1.469	0.019	−1.46	1,9,10,44	NGC 6638	−0.910	–	−0.91	1
NGC 5466	−1.922	0.051	−1.94	1,9,10,40	NGC 6642	−1.178	0.048	−1.22	1,2,5
NGC 5634	−1.840	0.057	−1.84	1,3,4,45	NGC 6656	−1.763	0.073	−1.66	1,3,25,54,85,86
NGC 5824	−1.962	0.089	−1.87	1,3,25,46,47	NGC 6712	−0.980	–	−0.98	1
NGC 5897	−1.915	0.055	−1.86	1,3,48	NGC 6715	−1.496	0.087	−1.45	1,9,25
NGC 5904	−1.260	0.030	−1.25	1,3,9,10,49,50	NGC 6717	−1.220	–	−1.22	1
NGC 5946	−1.342	0.115	−1.25	1,3,4	NGC 6723	−1.042	0.081	−1.06	1,10,87,88,89
NGC 5986	−1.538	0.015	−1.55	1,51	NGC 6779	−1.940	–	−1.94	1
NGC 6093	−1.726	0.020	−1.71	1,52	NGC 6864	−1.150	0.108	−1.25	1,3,4,90
NGC 6101	−1.940	–	−1.94	1	NGC 6934	−1.433	0.087	−1.43	1,91,92
NGC 6121	−1.121	0.042	−1.12	1,3,9,10,29,53,54,55,56,57,58,5	NGC 6981	−1.380	–	−1.38	1
NGC 6139	−1.583	0.031	−1.61	1,25,64	NGC 7006	−1.544	0.081	−1.48	1,3,25
NGC 6171	−0.980	0.028	−0.98	1,3,9,10	NGC 7078	−2.357	0.124	−2.33	1,3,8,9,10,93
NGC 6205	−1.512	0.023	−1.49	1,9,10	NGC 7089	−1.537	0.051	−1.61	1,7,8,9,10,94,95
NGC 6229	−1.307	0.117	−1.43	1,9,10,65	NGC 7099	−2.324	0.099	−2.23	1,70,83
NGC 6235	−1.240	–	−1.24	1	Pal 13	−1.820	0.118	−1.84	1,96,97
NGC 6266	−1.143	0.005	−1.14	1,66,67	Pal2	−1.380	–	−1.38	1
NGC 6273	−1.686	0.058	−1.70	1,68,69	Rup 106	−1.520	0.114	−1.64	1,3 25,98,99,100
NGC 6293	−1.950	–	−1.95	1	Ter 8	−2.139	0.064	−2.12	1,3,4,101

Notes. *The H10 catalogue values are transposed to match the $\log\epsilon Fe_{\odot} = 7.50$ solar composition by adding 0.04 dex.

References:1 Harris (2010); 2 Geisler et al. (2021); 3 Dias et al. (2016b); 4 Vásquez et al. (2018); 5 Geisler et al. (2023); 6 Carretta et al. (2013); 7 Pancino et al. (2017); 8 Kovalev et al. (2019); 9 Mészáros et al. (2020); 10 Horta et al. (2020); 11 Vargas et al. (2022); 12 Monty et al. (2023);
13 Koch-Hansen, Hansen & McWilliam (2021); 14 Marino et al. (2021); 15 Muñoz et al. (2021); 16 Carretta et al. (2011); 17 Gratton et al. (2012); 18 Marino et al. (2014b);
19 Yong, Grundahl & Norris (2015); 20 Tautvaišienė et al. (2022); 21 Baeza et al. (2022); 22 Dias et al. (2016b); 23 Cohen, Huang & Kirby (2011); 24 Mucciarelli et al. (2012);
25 Saviane et al. (2012); 26 Marino et al. (2014a); 27 Carretta (2015); 28 Wang et al. (2016); 29 Marino et al. (2017); 30 Cabrera-Ziri, Lardo & Mucciarelli (2019);
31 Carlos et al. (2023); 32 Muñoz, Geisler & Villanova (2013); 33 Simmerer et al. (2013); 34 Mucciarelli et al. (2015); 35 Magurno et al. (2018); 36 Marino et al. (2019);
37 Villanova et al. (2016); 38 Schaeuble et al. (2015); 39 Carretta et al. (2014b); 40 Lamb et al. (2015); 41 Boberg, Friel & Vesperini (2016); 42 Chun, Lee & Lim (2020);
43 Sbordone et al. (2015); 44 Givens & Pilachowski (2016); 45 Sbordone et al. (2015); 46 Roederer et al. (2016); 47 Mucciarelli et al. (2018);
48 Koch & McWilliam (2014); 49 Lai et al. (2011); 50 Gratton et al. (2013); 51 Johnson et al. (2017c); 52 Carretta et al. (2015); 53 Mucciarelli et al. (2011);
54 Marino et al. (2011); 55 Villanova & Geisler (2011); 56 Villanova et al. (2012); 57 Monaco et al. (2012); 58 D'Orazi et al. (2013);
59 Malavolta et al. (2014); 60 Spite et al. (2016); 61 MacLean et al. (2016); 62 Wang et al. (2017); 63 MacLean et al. (2018); 64 Bragaglia et al. (2015);
65 Johnson et al. (2017a); 66 Yong et al. (2014a); 67 Lapenna et al. (2015); 68 Johnson et al. (2015); 69 Johnson et al. (2017b); 70 Cohen (2011);
71 Souza et al. (2023); 72 Mucciarelli et al. (2016); 73 Massari et al. (2017); 74 Johnson et al. (2016); 75 Puls et al. (2018); 76 Johnson et al. (2019);
77 Hanke et al. (2017); 78 Bragaglia et al. (2017); 79 Barbuy et al. (2018); 80 Ernandes et al. (2018) 81 Valenti, Origlia & Rich (2011); 82 Johnson et al. (2018);
83 O'Malley & Chaboyer (2018); 84 Villanova et al. (2017); 85 Roederer, Marino & Sneden (2011); 86 McKenzie et al. (2022); 87 Gratton et al. (2015);
88 Rojas-Arriagada et al. (2016); 89 Crestani et al. (2019); 90 Kacharov, Koch & McWilliam (2013); 91 Marino et al. (2018); 92 Marino et al. (2021);
93 Worley et al. (2013); 94 Yong et al. (2014b); 95 Lardo, Mucciarelli & Bastian (2016); 96 Bradford et al. (2011); 97 Koch & Côté (2019); 98 Villanova et al. (2013);
99 Frelijj et al. (2021); 100 Lucertini et al. (2022); 101 Carretta et al. (2014a).

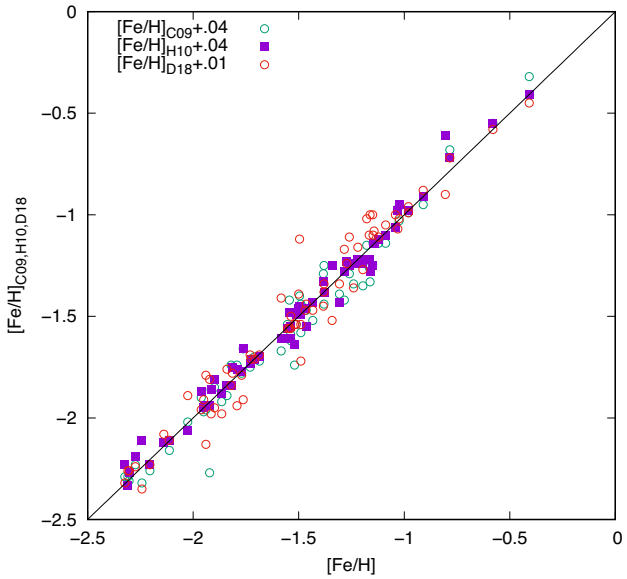

Figure 1. Comparison of the compiled, solar composition standardized ($\log\epsilon(\mathrm{Fe})_\odot = 7.50$) [Fe/H] values of GCs with the metallicities of Carretta et al. (2009), the 2010 edition of the Harris (1996) catalogue, and the second data release of the compilation of B. Dias (Dias et al. 2015, 2016a, b; Vásquez et al. 2018). The latter has an average offset of 0.03 dex compared to the H10 scale.

2.3 Photometric data

The *G* band time-series data of RRab stars published in the third data release (DR3) of the *Gaia* collaboration Gaia Collaboration (2016, 2022) are utilized.

The positions of variable stars given in the C. Clement catalogue (Clement et al. 2001, hereafter CC01)[1] are cross-correlated with the Gaia DR3 positions to get the epoch-photometry data of RRLs in GCs. We find time-series data within 1 arcsec position match for 2694 stars. The LCs contain 20−100 data points, typically. Known RRLs and stars of uncertain variable classification are checked visually one-by-one to select RRab stars of reliable Fourier solution using the MUFRAN (Kolláth 1990) programme. Each LC is fitted by appropriate order Fourier sums. In order to avoid unreliable bumps of the Fourier fits of gappy and/or poor data, a few (1–3) artificial points are interpolated to stabilize the solution in some cases. Data points with error flag '1' are removed only if they are indeed discrepant.

The LCs are categorized according to their scatter and the reliability of the fit. Good-quality LCs (Sample A) are fitted with at least fifth-order Fourier sums, and they do not show any considerable scatter or sign of the Blazhko effect. Exceptions are V202 in NGC 5272, V44 in NGC 6864, and V28 in NGC 7089; these stars are long-period, small-amplitude variables with sinusoidal-shape LCs, which are fitted with third-order Fourier sums. The minimum order of the fit for poor-quality LCs (Sample B) is 4. The LCs of these stars are scattered or gappy, many of them are known to show the Blazhko modulation. Variables with unreliable fits and atypical-shape LCs suggesting other types of variability are not used.

We have removed from the sample variables identified as probable field stars (f, f?) in the CC01 catalogue only if their mean magnitudes are discrepant, because this information in the catalogue is not always reliable.

[1] http://www.astro.utoronto.ca/ cclement/cat/listngc.html

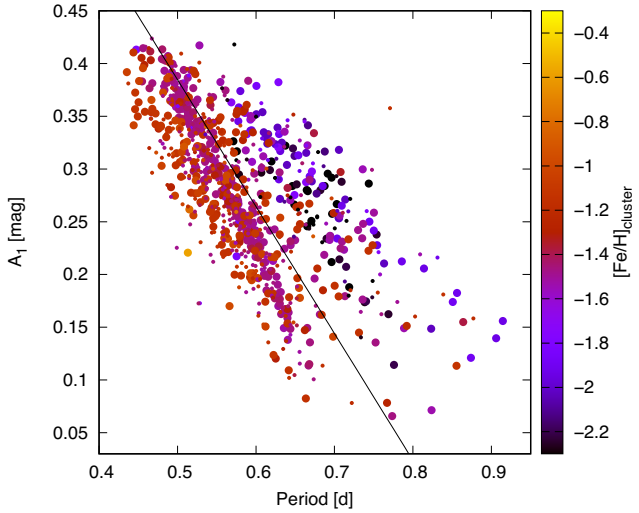

Figure 2. The *Period−amplitude* (Fourier A_1 amplitude) Bailey-diagram of RRab stars of Sample A (large dots) and Sample B (small dots) is shown. The colour-code denotes the spectroscopic metallicity of the cluster the variable belongs to. The black line in the figure separates variables supposed to have Oo-type I and Oo- type II properties.

Finally, we selected 526 good- (Sample A) and 396 poor-quality (Sample B) RRab LCs belonging to 70 GCs. The variables of Sample A belong to 64 GCs.

The distribution of the variables in the clusters is very unequal, there are clusters with only 1–2 RRLs, while LCs of 139 variables are utilized in the GC M3.

3 PHOTOMETRIC METALLICITY FORMULAE

To derive relations between the LC parameters of RRab stars and the mean spectroscopic [Fe/H] values of the clusters only the best-quality LCs (Sample A) are used.

The Gaia LC parameters indicate a very strong linear correlation between the [Fe/H] and the period and the φ_{31} phase parameter, similarly to the *V* band results published in Jurcsik & Kovács (1996). We also detect that the results systematically overestimate the [Fe/H] towards metal-poor clusters as in our previous study. Neither the overall accuracy of the fit nor the systematics of the differences could be improved using non-linear and/or multiparameter formulae.

Different selection criteria are applied to remove the outliers, however, the standard error of the fit cannot be decreased below 0.15−0.16 dex reliably. It was shown in Jurcsik, Hajdu & Juhász (2021) that both the *V* band (Jurcsik & Kovács 1996) and the *I* band (Smolec 2005) metallicity formulae yield systematically different [Fe/H] values for the OoI- and OoII-type variables (which are supposed to be more evolved stars) in the same cluster. Therefore, we check the fitting accuracy for Oo-type I and Oo-type II variables separately. Instead of separating the GCs according to their Oo types, the Oo types of the variables are determined based on their positions on the *period−amplitude* (Bailey) diagram. The *period*−A_1 plot of the total sample of stars is shown in Fig. 2. Here, we use the first-order Fourier amplitude, A_1, as the total amplitude cannot be determined reliably enough for sparse data in some cases. It is somewhat arbitrary where to separate the two Oo types, therefore we have tested different linear and quadratic solutions for the separator line. However, no significant differences in the final results emerged depending on the choice of the separator.

We adopt equation (1), shown as black line in Fig. 2, to divide the Oo types in the total sample of variables used.

$$A_1(G) = -1.203P + 0.986. \quad (1)$$

Using equation (1), Sample A is separated to 318 Oo-type I and 208 Oo-type II variables.

The rms of the residuals of the total Sample A when skipping outliers in successive steps using 3σ and 2.5σ thresholds are 0.160 and 0.149 dex respectively. However, the 3σ limit is about 0.45 dex, which is too high compared to the full range of the [Fe/H] values of the GCs. Using 2.5σ does not improve the fit significantly, but it seems to narrow the range of the residuals artificially, especially when the different Oo types are fitted separately. Therefore, we have decided to use fixed selection limits to cut the outliers. Stars with deviations larger than 0.6, 0.5, and 0.4 dex are removed in successive steps. This process resulted in the selection of 1 per cent − 3 per cent of the variables as outliers in the different samples.

In the course of checking the outliers to explain their anomalous behaviour, it has been noticed that the photometric metallicity of two of the tree variables in NGC 6316 (V15, V18) underestimate the spectroscopic value significantly, while the Gaia proper-motion values of the third variable (V17) contradict its cluster membership status. Based on *HST* observations, Deras et al. (2023) have concluded in a recent paper that the cluster metallicity should be significantly lower than given in the Harris (2010) catalogue. No published HRS [Fe/H] data of this cluster is available. Therefore, we decided to remove this cluster from the calibrating sample.

Finally, the following linear formulae have been derived. Note, that the φ_{31} phase differences correspond to sine series decomposition.

Sample A, 63 GCs, 511 stars, 12 outliers, rms = 0.152 dex:

$$[\mathrm{Fe/H}]_{\mathrm{phot}} = -5.716(.130)P + 1.019(.027)\varphi_{31} - 3.504(.097). \quad (2)$$

Outliers: V54/IC 4499, V11/NGC 1851, V3, V10/NGC 5053, V3/NGC 6171, V228/NGC 6266, V1/NGC 6293, V8/NGC 6453, V6/NGC 6541, V27/NGC 6981, V28/NGC 7089, and V4/Pal13.

Sample A, Oo-type I, 30 GCs, 313 stars, 3 outliers, rms = 0.114 dex:

$$[\mathrm{Fe/H}]_{\mathrm{phot}} = -4.373(.196)P + 0.736(.031)\varphi_{31} - 2.768(.100). \quad (3)$$

Outliers: V3/NGC 5053, V6/NGC 6541, and V4/Pal13.

Sample A, Oo-type II, 51 GCs, 200 stars, 7 outliers, rms = 0.169 dex:

$$[\mathrm{Fe/H}]_{\mathrm{phot}} = -7.212(.248)P + 1.353(.048)\varphi_{31} - 4.324(.157). \quad (4)$$

Outliers: V54/IC 4499, V10/NGC 5053, V202/NGC 5272, V1/NGC 6293, V8/NGC 6453, V27/NGC 6981, and V28/NGC 7089.

The goodness of the fits using more parameters and/or non-linear formulae are very similar. There is no formula which would yield a residual scatter better than 0.148 dex using the data set equation (2) has been defined on.

The outlier stars are investigated separately to explain their anomalous $[\mathrm{Fe/H}]_{\mathrm{phot}}$ values. It is found that: V54/IC 4499, V11/NGC 1851, and V27/NGC 6981 are long-period variables with large amplitudes; V10/NGC 5053, V202/NGC 5272, V228/NGC 6266, and V28/NGC 7089 are also long-period variables but with very low amplitudes; V3/NGC 5053 is the shortest period RRab in the cluster, its total amplitude is 0.2 mag smaller than the amplitude of V1, the next shortest period RRab at a 0.05 d longer period in this cluster; V8/NGC 6453 is 0.3 mag brighter and its LC shape is markedly different from the similar-period V4 in the cluster; V3/NGC 6171: its amplitude is 0.2 mag smaller than the other Oo-type I variables with similar periods in the cluster; V4/Pal13: there are two good LCs in the cluster (V3 and V4). Based on their periods and amplitudes they are Oo-type I RRLs, however, despite their similar periods, V4 is 0.1 mag fainter than V3 and and its total amplitude is 0.2 mag smaller; V6/NGC 6541: its 0.45 d period is anomalously short for a cluster with [Fe/H] = −1.77. V1/NGC 6293: there is no other RRL LC in this cluster to compare.

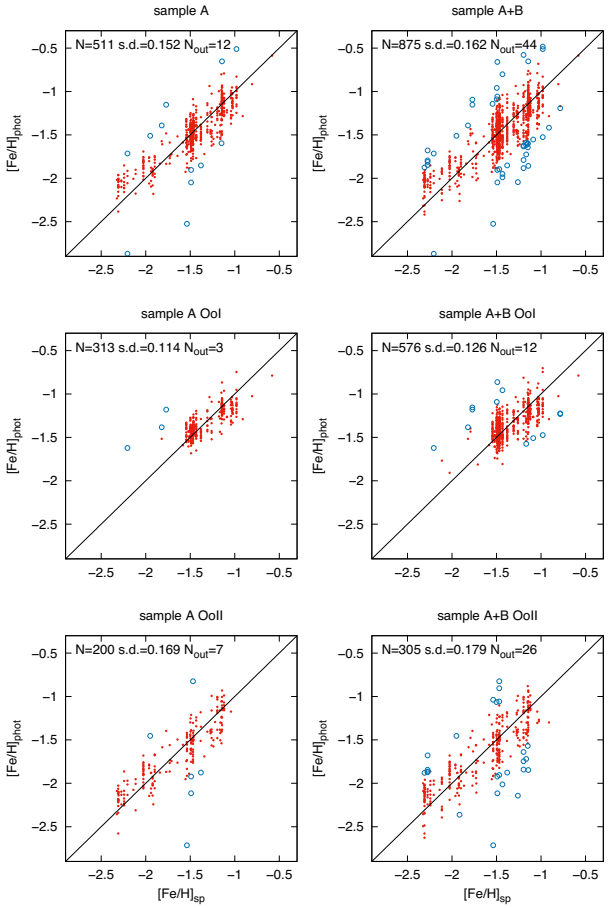

Figure 3. Comparison of the Gaia *G* band photometric and the spectroscopic [Fe/H] values of GC RRab stars. The left-hand panels show the results for the best quality LCs (Sample A). The top-, middle-, and bottom-left-hand panels show the results for the complete Sample A, its Oo-type I, and Oo-type II sub-samples applying equations (2), (3), and (4), respectively. The results of the combined sample of good and poor quality LCs (Sample A + Sample B) are shown in the right-hand panels of the figure. Removed outliers are indicated by open circles in each plot. The statistical properties of the fits are given near the top of each panel.

Summarizing, most of these stars have extremely short or long periods compared to the bulk of the cluster variables, and their amplitudes are anomalously large or small. The others show differing LC characteristics and/or mean brightness in comparison with similar period stars in the given cluster. Eight of the 13 selected outliers are Oo-type II variables based on their periods and amplitudes.

The photometric metallicities versus the mean cluster spectroscopic [Fe/H] values are shown for Sample A and for Sample A + B in the left-hand and right-hand panels of Fig. 3. Outliers are shown by open circles, these stars are used neither in deriving the metallicty formulae, nor in calculating the mean cluster values. The top, middle, and bottom panels document the results applying equations (2), (3), and (4) using the LC parameters of the full samples and on its Oo-type I and Oo-type II sub-samples, respectively. The LCs of Sample

B might be biased by Blazhko modulation and/or data sparseness or scatter, this is the reason for the large number of the outliers in these plots. However, the overall agreement with the spectroscopic data is also evident in the right-hand panels of Fig. 3, indicating that the photometric metallicity estimates work relatively well on LCs of poor quality, too.

The Oo-type I sample covers only about the half of the total [Fe/H] range of the clusters, meaning that equation (3) is valid only in the $-0.9 > [Fe/H] > -1.5$ range. However, the significant decrease of the rms of the residuals between Sample A and its Oo-type I part arises not only from the narrow [Fe/H] range but also from the omission of the RRab stars with Oo-type II properties from this sample. The scatter of the OoI-type stars in the middle left-hand panel of Fig. 3 is smaller than in this part of the plot shown in the top panel.

This is in contrast with the results for the Oo-type II sample (bottom panels in Fig. 3). The separation of the Oo types does not improve the fitting accuracy in this case, the rms of the fit is even larger than for the total sample. This is in line with the outliers preferably being Oo-type II variables. Although Oo-type II variables are less numerous than Oo-type I stars, there are about 2–3 times as many outliers detected in this sample, compared to the Oo-type I variables.

The Oo-type II sample covers nearly the full metallicity range of the used GCs, and this solution yields a better agreement with the spectroscopic data at the metal-poor end than the results using equation (2). The mean differences between the $[Fe/H]_{phot}$ and $[Fe/H]_{sp}$ values for the 10 clusters with $[Fe/H] < -1.95$ dex are 0.19 and 0.11 dex when using equations (2) and (4), respectively.

The panels in Fig. 4 show the results for the mean cluster values in a similar plot as in Fig. 3. The circles size is scaled to reflect the number of variables used to derive the mean value of $[Fe/H]_{phot}$. The error bars indicate the rms scatter of the spectroscopic and photometric [Fe/H] values. Note that small (zero) errors do not necessarily indicate high-accuracy, because single photometric or spectroscopic data are shown by zero error.

The $[Fe/H]_{phot}$ values derived for sample A and for the total sample of variables (Sample A + Sample B) are given in Table 2. The metallicities are calculated both by using equation (2) for each variable of the samples, and by using equations (3) and (4) depending on the Oo-type of the stars.

The mean metallicities derived for the calibrating sample (Sample A) and for the total sample including also poor-quality LCs (Sample A + Sample B) do not show any significant differences. This is partly in line with the results of Dékány, Grebel & Pojmański (2021) and Dékány & Grebel (2022), who concluded that the exclusion of the Blazhko stars did not result any improvement of the photometric metallicity models in the Johnson-Cousins *I* and the Gaia *G* photometric bands. However, the benefit of our choice of excluding poor and scattered LCs from the calibrating sample of the metallicity formula is documented in Fig. 5. This figure compares the $[Fe/H]_{sp} - [Fe/H]_{phot}$ values using equation (2) and a similar two-parameter formula defined on the combined total sample (Sample A + Sample B). The systematics of the differences are similar in the two cases, however, when using the combined sample for the calibration the systematic differences tend to be larger than when only the good-quality LCs are utilized.

4 RESULTS ON PECULIAR CLUSTERS

4.1 ω Cen

We have found 31 and 8 good- and poor-quality LCs in ω Cen, respectively, in the Gaia DR3 *G* band time-series data, which are

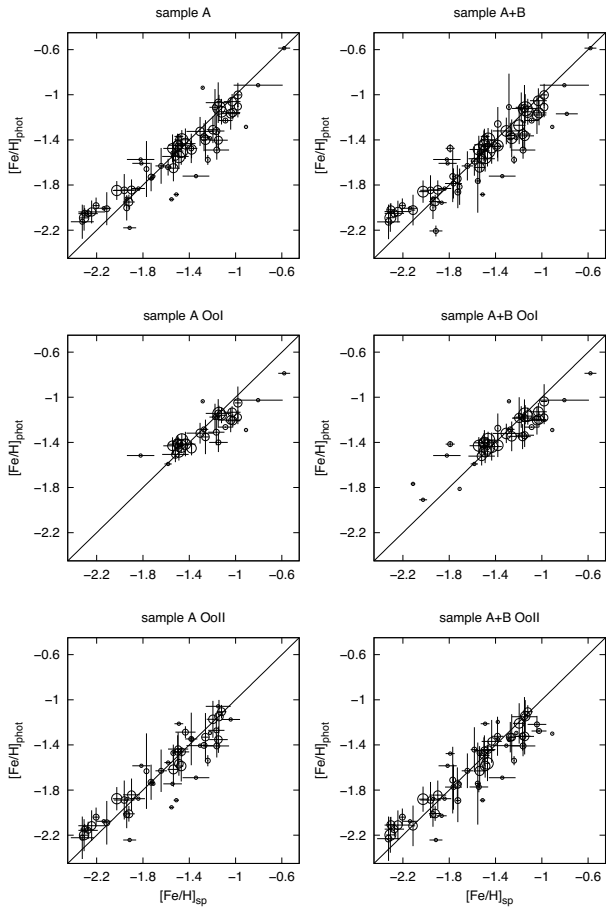

Figure 4. The same panels are shown for the cluster mean values as in Fig. 3. The circles size is scaled according to the number of LCs used to derive the mean photometric [Fe/H] value. Error-bars correspond to the dispersion of the $[Fe/H]_{phot}$ and $[Fe/H]_{sp}$ values that the means are calculated from.

suitable to estimate their $[Fe/H]_{phot}$ values. The results are compared with the spectroscopic [Fe/H] measured by Sollima et al. (2006) and Magurno et al. (2019), and with the metallicities estimated from *period−luminosity−metallicity*-relation by Bono et al. (2019) in Fig. 6. The 0.00 and 0.04 dex overall shifts between the data correspond to the differences between the reference solar iron abundances for the Magurno et al. (2019) and Bono et al. (2019) data, respectively, while the −0.1 dex shift of the [Fe/H] values given in Sollima et al. (2006) refers to the mean difference obtained from the data.

Taking into account the large uncertainties of most of the literature data, and the uncertainty of the LC parameters of some of the RRLs we use, the agreement between our and previous results is satisfactory. Significant differences are detected only in a few cases, and the differences between the literature data of the same star (these data have the same $[Fe/H]_{phot}$ values, i.e. they lay along a horizontal line in Fig. 6) are of similar size to their differences from the photometric [Fe/H] values.

The distributions of the obtained metallicty values using equations (2), (3), and (4) on the total, the OoI, and the OoII subsamples, respectively, are shown in the panels of Fig. 7. The [Fe/H] bins around −1.90, −1.30, and −1.90 are the most populated bins in the three samples, respectively.

The [Fe/H] distribution shown for the total sample in Fig. 7 is very similar to the distribution detected from spectroscopic measurements

Table 2. Results on the mean photometric [Fe/H] values of the GCs.

Cluster		Sample A						Sample A + Sample B					
	$[Fe/H]_{sp}$	$[Fe/H]_{phot}^{equation(2)}$	Disp.	N	$[Fe/H]_{phot}^{equation(3),(4)}$	Disp.	N	$[Fe/H]_{phot}^{equation(2)}$	Disp.	N	$[Fe/H]_{phot}^{equation(3),(4)}$	Disp.	N
Arp2	−1.710	−1.722	–	1	−1.744	–	1	−1.815	0.161	2	−1.778	0.049	2
Djo2	−0.805	−0.915	–	1	−1.026	–	1	−0.915	–	1	−1.026	–	1
IC 4499	−1.490	−1.551	0.107	31	−1.508	0.093	31	−1.555	0.126	47	−1.510	0.130	48
NGC 362	−1.166	−1.322	0.141	5	−1.294	0.115	5	−1.349	0.124	11	−1.359	0.113	12
NGC 1261	−1.272	−1.376	0.124	5	−1.356	0.067	5	−1.361	0.113	9	−1.297	0.133	9
NGC 1851	−1.148	−1.403	0.083	7	−1.365	0.106	8	−1.364	0.123	13	−1.307	0.160	14
NGC 1904	−1.553	−1.927	–	1	−1.952	–	1	−1.764	0.282	2	−1.637	0.445	2
NGC 2298	−1.865	–	–	0	–	–	0	−1.956	–	1	−2.028	–	1
NGC 2419	−2.113	−2.010	0.146	3	−2.090	0.193	3	−2.022	0.136	10	−2.090	0.209	10
NGC 2808	−1.088	−1.228	0.018	2	−1.265	0.002	2	−1.228	0.015	2	−1.265	0.002	2
NGC 3201	−1.464	−1.399	0.086	43	−1.387	0.060	43	−1.398	0.104	70	−1.383	0.084	70
NGC 4147	−1.792	–	–	0	–	–	0	−1.475	0.037	3	−1.436	0.040	3
NGC 4590	−2.274	−2.054	0.041	3	−2.157	0.077	3	−2.051	0.035	5	−2.140	0.068	5
NGC 4833	−1.899	−1.844	0.094	7	−1.842	0.144	7	−1.843	0.084	9	−1.846	0.125	9
NGC 5024	−2.026	−1.848	0.083	19	−1.876	0.103	19	−1.859	0.099	23	−1.885	0.118	23
NGC 5053	−2.205	−1.982	0.071	3	−2.039	0.084	3	−1.982	0.064	3	−2.039	0.084	3
NGC 5272	−1.469	−1.499	0.122	55	−1.471	0.106	54	−1.497	0.139	138	−1.468	0.124	135
NGC 5466	−1.922	−1.950	0.065	7	−2.010	0.069	7	−1.947	0.061	9	−2.006	0.067	9
NGC 5634	−1.840	−1.831	–	1	−1.877	–	1	−1.831	–	1	−1.877	–	1
NGC 5824	−1.962	−1.847	0.144	4	−1.888	0.173	4	−1.847	0.133	4	−1.888	0.173	4
NGC 5897	−1.915	−2.180	–	1	−2.243	–	1	−2.207	0.048	2	−2.243	–	1
NGC 5904	−1.260	−1.400	0.174	12	−1.341	0.177	12	−1.387	0.168	19	−1.340	0.153	19
NGC 5946	−1.342	−1.721	–	1	−1.690	–	1	−1.721	–	1	−1.690	–	1
NGC 5986	−1.538	−1.519	0.064	2	−1.472	0.075	2	−1.519	0.052	2	−1.472	0.075	2
NGC 6093	−1.726	−1.741	–	1	−1.732	–	1	−1.862	0.144	3	−1.947	0.193	3
NGC 6101	−1.940	−2.002	0.112	3	−2.017	0.121	3	−2.002	0.100	3	−2.017	0.121	3
NGC 6121	−1.121	−1.150	0.114	22	−1.143	0.071	22	−1.151	0.115	28	−1.155	0.081	28
NGC 6139	−1.583	−1.641	0.075	2	−1.574	0.025	2	−1.588	0.130	3	−1.453	0.210	3
NGC 6171	−0.980	−1.001	0.108	7	−1.050	0.145	8	−1.001	0.098	9	−1.028	0.165	11
NGC 6205	−1.512	−1.884	–	1	−1.890	–	1	−1.884	–	1	−1.890	–	1
NGC 6229	−1.307	−1.325	0.128	9	−1.328	0.091	9	−1.321	0.118	22	−1.325	0.086	22
NGC 6235	−1.240	−1.577	0.044	2	−1.539	0.050	2	−1.577	0.036	2	−1.539	0.050	2
NGC 6266	−1.143	−1.115	0.115	53	−1.144	0.085	54	−1.124	0.129	87	−1.158	0.102	88
NGC 6273	−1.643	−1.630	0.159	2	−1.629	0.188	2	−1.630	0.130	2	−1.629	0.188	2
NGC 6333	−1.730	−1.729	0.126	3	−1.730	0.156	3	−1.744	0.120	6	−1.763	0.165	6
NGC 6341	−2.304	−2.049	0.046	3	−2.146	0.046	3	−2.019	0.058	7	−2.089	0.074	7
NGC 6355	−1.383	−1.475	0.130	2	−1.347	0.233	2	−1.455	0.103	3	−1.308	0.178	3
NGC 6362	−1.024	−1.158	0.062	8	−1.208	0.059	8	−1.161	0.110	16	−1.201	0.077	16
NGC 6366	−0.580	−0.586	–	1	−0.788	–	1	−0.586	–	1	−0.788	–	1
NGC 6401	−1.030	−1.061	0.068	9	−1.133	0.054	9	−1.052	0.109	15	−1.127	0.092	15
NGC 6402	−1.196	−1.309	0.119	9	−1.173	0.164	9	−1.270	0.167	24	−1.210	0.185	26
NGC 6426	−2.243	−2.039	0.101	8	−2.115	0.136	8	−2.035	0.096	9	−2.105	0.131	9
NGC 6453	−1.490	−1.369	–	1	−1.212	–	1	−1.369	–	1	−1.212	–	1
NGC 6535	−1.814	−1.608	–	1	−1.585	–	1	−1.608	–	1	−1.585	–	1
NGC 6541	−1.770	−1.658	0.248	2	−1.633	0.335	2	−1.724	0.228	3	−1.764	0.328	3
NGC 6558	−1.162	−1.489	0.086	3	−1.409	0.102	3	−1.489	0.077	3	−1.409	0.102	3
NGC 6569	−0.784	–	–	0	–	–	0	−1.169	–	1	–	–	0
NGC 6584	−1.500	−1.451	0.107	15	−1.421	0.094	15	−1.453	0.138	22	−1.435	0.132	21
NGC 6626	−1.284	−0.938	–	1	−1.036	–	1	−1.108	0.296	2	−1.195	0.226	2
NGC 6638	−0.910	−1.284	–	1	−1.290	–	1	−1.284	–	1	−1.295	0.007	2
NGC 6642	−1.178	−1.111	0.162	2	−1.175	0.118	2	−1.111	0.132	2	−1.175	0.118	2
NGC 6656	−1.763	–	–	0	–	–	0	−1.786	0.134	2	−1.774	0.200	2
NGC 6712	−0.980	−1.104	0.097	5	−1.177	0.062	5	−1.109	0.089	6	−1.185	0.058	6
NGC 6715	−1.496	−1.447	0.100	17	−1.421	0.087	17	−1.443	0.141	30	−1.407	0.131	31
NGC 6717	−1.220	−1.385	–	1	−1.294	–	1	−1.385	–	1	−1.294	–	1
NGC 6723	−1.042	−1.167	0.142	10	−1.199	0.102	10	−1.179	0.168	14	−1.212	0.134	14
NGC 6779	−1.940	−1.921	–	1	−1.880	–	1	−1.921	–	1	−1.880	–	1
NGC 6864	−1.150	−1.070	0.180	5	−1.126	0.116	5	−1.121	0.208	7	−1.204	0.186	8
NGC 6934	−1.433	−1.433	0.134	23	−1.398	0.111	23	−1.460	0.152	43	−1.443	0.145	44
NGC 6981	−1.380	−1.484	0.079	14	−1.445	0.066	14	−1.451	0.139	22	−1.408	0.119	22
NGC 7006	−1.544	−1.476	0.124	16	−1.450	0.107	16	−1.485	0.122	27	−1.454	0.121	28
NGC 7078	−2.309	−2.092	0.113	13	−2.199	0.141	13	−2.089	0.125	24	−2.196	0.170	24

Table 2 – *continued*

Cluster	Sample A							Sample A + Sample B					
	$[Fe/H]_{sp}$	$[Fe/H]_{phot}^{equation(2)}$	Disp.	N	$[Fe/H]_{phot}^{equation(3),(4)}$	Disp.	N	$[Fe/H]_{phot}^{equation(2)}$	Disp.	N	$[Fe/H]_{phot}^{equation(3),(4)}$	Disp.	N
NGC 7089	−1.537	−1.651	0.116	11	−1.617	0.153	11	−1.644	0.144	13	−1.642	0.170	12
NGC 7099	−2.324	−2.126	0.151	2	−2.222	0.188	2	−2.127	0.153	4	−2.235	0.229	4
Pal 13	−1.820	−1.574	–	1	−1.517	–	1	−1.574	–	1	−1.517	–	1
Pal2	−1.380	–	–	0	–	–	0	−1.259	0.150	4	−1.255	0.114	4
Rup 106	−1.520	−1.547	0.102	6	−1.507	0.068	6	−1.567	0.117	11	−1.529	0.092	11
Ter8	−2.139	−2.006	–	1	−2.076	–	1	−2.006	–	1	−2.076	–	1

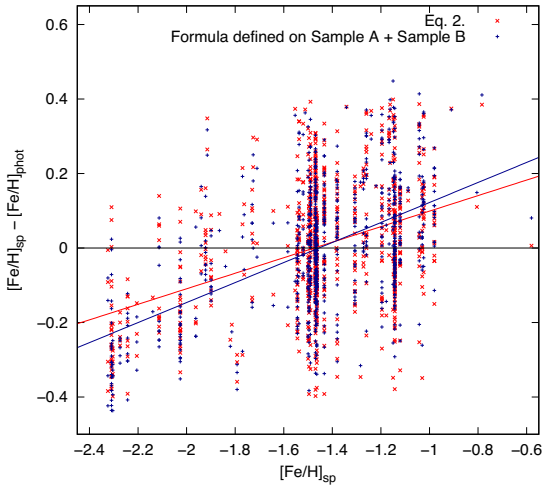

Figure 5. Comparison of the result using equation (2), and according to a formula that is calibrated on the combined Sample A + Sample B. The systematic differences of the results are evident in both cases, but its amplitude is smaller when equation (2) is applied.

by Magurno et al. (2019, see their figure 8). There is a prominent peak at around −1.8 to −1.9 dex and both the more metal-poor and less metal-poor tails are populated. The photometric results also reveal that the higher metallicity RRLs are Oo-type I stars (the LC of the only exception is uncertain), while RRLs in the most metal-poor group are Oo-type II variables. The main sample of the variables belongs to the OoII class.

4.2 Oo-type III clusters and 47 Tuc

Photometric studies of RRLs in Oo-type III GCs showed that these long-period and metal-rich variables do not yield reliable photometric metallicity values using formulae calibrated on the LCs of Galactic field RRLs (see e.g. Pritzl et al. 2002). Therefore, it is an open question whether these stars obey another photometric metallicity relation, or there is no connection between their [Fe/H] and LC parameters.

Gaia DR3 provides LCs of RRLs in NGC 6304, NGC 6388, and NGC 6441, however, many of them are of very poor-quality and/or their Gaia proper motion values contradict their cluster membership (Vasiliev & Baumgardt 2021; Gaia Collaboration 2022). The probable cluster members in NGC 6441 with good- and poor-quality Gaia LCs are V37, V38, V39, V96, and V43, V46, V52, V61, V66, respectively. The shapes of the LCs of V96 and V52 are, however atypical for RRL stars. The probable members in NGC 6388 are V21, V28 (good), and V22, V58 (poor) but the membership status of V28 and V22 are questionable. We did not find Gaia RRL time-series data of any probable clusters member in NGC 6304.

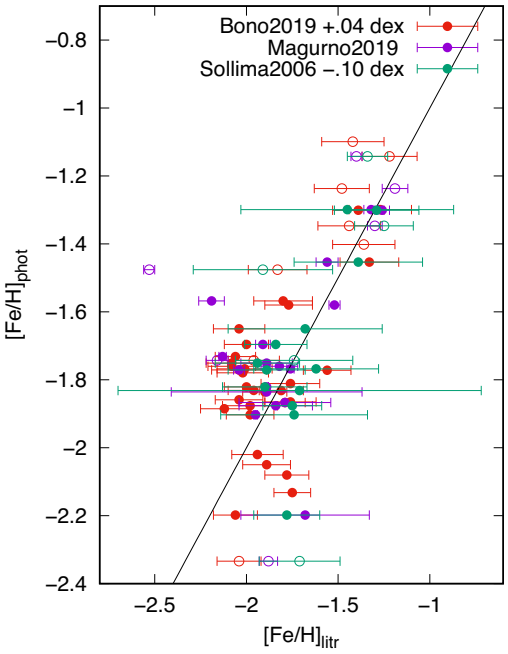

Figure 6. Comparison of the photometric and the literature [Fe/H] values of RRab stars in ω Cen. The literature data are taken from the spectroscopic studies of Sollima et al. (2006) and Magurno et al. (2019) and are the values derived from *period*−*luminosity*−*metallicity*-relation (Bono et al. 2019). The $[Fe/H]_{phot}$ values are calculated according to equation (2). Open symbols refer to the results obtained from poor-quality LCs. The black line is the identity function. Taking into account the uncertainties, the agreement is satisfactory. The 0.04 dex offset of the Bono et al. (2019) data corresponds to the differences of the solar reference values used. There is a −0.1 dex mean difference in comparison with the results of the data published by Sollima et al. (2006) that should have some other origin.

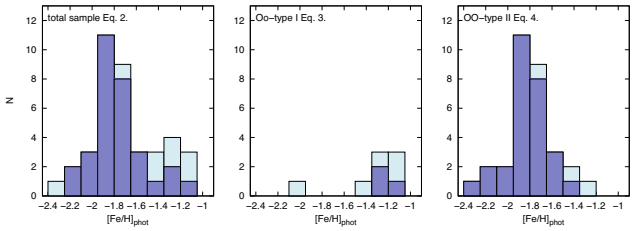

Figure 7. The histograms of the derived $[Fe/H]_{phot}$ values for ω Cen RRab stars are shown. The dark- and the light-blue columns correspond to the results obtained for the good- and the poor-quality LCs, respectively. The left-hand panel documents the distribution of the $[Fe/H]_{phot}$ values for the total sample of the variables in the cluster using equation (2). The middle and right-hand panels are the results for the OoI- and OoII-type stars calculated according to equations (3) and (4), respectively.

Accordingly, these data are not adequate neither in number nor in quality to establish a relation between the cluster metallicities and the LC parameters.

Moreover, another problem arises from that, that the $[Fe/H]_{sp}$ values of these clusters are very similar −0.41, −0.51, and −0.42 for NGC 6304, NGC 6388, and NGC 6441, respectively [Harris 2010, transformed to $\log\epsilon(Fe)_{\odot} = 7.50$]. As a result, a direct approach to find an appropriate formula to fit their [Fe/H] would lead to degeneracy, yielding coefficients of the LC parameters close to zero and a constant term equalling the mean metallicity of the clusters.

The only RRL star in 47 Tuc, V9, a long-period and large-amplitude variable also in a metal-rich cluster, which however is about 0.3 dex less metal-rich than the three Oo-type III clusters are, was proposed to be a close analogue to the RRLs in NGC 6388 and NGC 6441 by Pritzl et al. (2000). The photometric [Fe/H] derived for V9 using any of the formulae defined in Section 3 is 0.8−1.0 dex more metal-poor than the spectroscopic metallicity of the cluster. Trying to find a common [Fe/H] – LC parameter solution using V9/47 Tuc and the OoIII-type RRLs has, however, also failed.

Supposing that some of the outliers listed in Section 3 might also belong to the OoIII type, it is checked whether the addition of these stars would help to fit the $[Fe/H]_{sp}$ with LC parameters. However, this trial has not led to success either.

Thus, we conclude that in order to answer the question whether there is any photometric metallicity formula valid for these peculiar RRL stars, more data on a wider [Fe/H] range of similar variables are needed. Unfortunately, there are very few long-period but relatively metal-rich field RRab stars with HRS [Fe/H] determinations (e.g. XZ Gru, HK Pup, and AX Leo), and the similarity of these stars to the variables in the OoIII clusters might be questioned. Moreover, the significant differences between the populations of the Oo types in the Galactic field and GC samples as discussed by e.g. Fabrizio et al. (2021) warns that the Oo classification scheme may not hold for Galactic field stars. Therefore, to extend the OoIII type sample significantly is unrealistic at present.

5 COMPARISON WITH OTHER $[FE/H]_{PHOT}$ RESULTS

The RR Lyr LC parameters and metallicities available in the Gaia DR3 archive are compared with the LC parameters and the $[Fe/H]_{phot}$ values derived in Section 3 for the GC NGC 5272 (M3) in Fig. 8.

The cross-matching of the Gaia DR3 epoch photometry data with the CC01 catalogue of variables provides LCs of 163 RRab stars in M3. As a result of the one-by-one analysis we selected 55 good- and 84 poor-quality LCs from this sample and no reliable Fourier solution was obtained for 24 stars. The Fourier parameters and the derived [Fe/H] values using equation (2) of the good and the poor LCs are shown by filled and open blue circles in Fig. 8, respectively. For comparison, the LC parameters and the metallicities of 158 RRab stars provided by the Gaia DR3 (Clementini et al. 2022) are plotted as cross marks. These $[Fe/H]_{phot}$ values are calculated according to the non-linear formula of Nemec et al. (2013) transformed to the Gaia *G* band magnitudes.

The largest differences between the DR3 and the recent results are in the photometric metallicities. The Nemec et al. (2013) formula yields significantly less reliable metallicities than the formulae given in Section 3. The differences in the peak to peak amplitude and the Fourier parameters are less significant, part of the differences arises from the omission of 24 LCs with unreliable Fourier solutions in our sample, but the parameters of many stars in common differs also, especially for noisy or Blazhko-star data (poor LCs). The Gaia

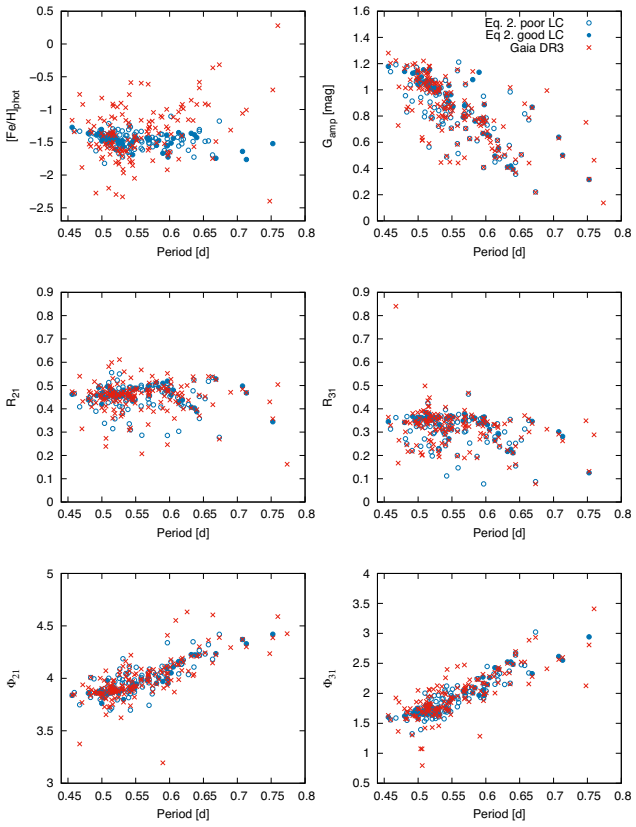

Figure 8. Comparison of the $[Fe/H]_{phot}$ values and the LC parameters of RRab stars in NGC 5272 (M3) derived in this paper (filled and open blue circles for good- and poor-quality LCs, respectively) and as given by the Gaia DR3 RRL pipeline (Clementini et al. 2022; red crosses).

pipeline detects most of the RRab stars correctly, but e.g, V42, a non-modulated large-amplitude (1.1 mag) variable with a good-quality epoch photometry available in Gaia DR3, is not included in the catalogue of RRL variables (Clementini et al. 2022). The different number of RRab stars in our and in the Gaia DR3 RRL samples indicates that there are five RRab variables that were not identified as such by the RRL pipeline.

Photometric metallicities of RRL stars using Gaia *G* band LC of the DR2 and DR3 archives were published in Iorio & Belokurov (2021), Dékány & Grebel (2022), and Li et al. (2023). These results for GC RRab stars and the $[Fe/H]_{phot}$ values calculated according to equation (2), and equations (3) - (4) are compared with the spectroscopic cluster metallicities, listed in Table 1, in Fig. 9. For completeness, we also show the results obtained using one of the recent *V* band formulae (Mullen et al. 2021). However, we note that the comparison from different bands needs additional transformations of the involved parameters, which might not be known accurately enough.

Using the parameters of the 508 good-quality LCs (Sample A minus the outliers listed in Section 3) the clusters mean $[Fe/H]_{phot}$ values are calculated according to the formulae derived by Iorio & Belokurov (2021) and Li et al. (2023) in panels (a) and (c). Dékány & Grebel (2022) did not give an explicit metallicity formula, instead they published the $[Fe/H]_{phot}$ values of over 60 000 Galactic RRL stars. Cross-correlating their catalogue with the CC01 catalogue we find 618 common stars. Panel (b) in Fig. 9 displays the mean cluster $[Fe/H]_{phot}$ values calculated from the metallicties published by Dékány & Grebel (2022) for these stars. The results using equation (2) and by applying equations (3) and (4) on the LC parameters of

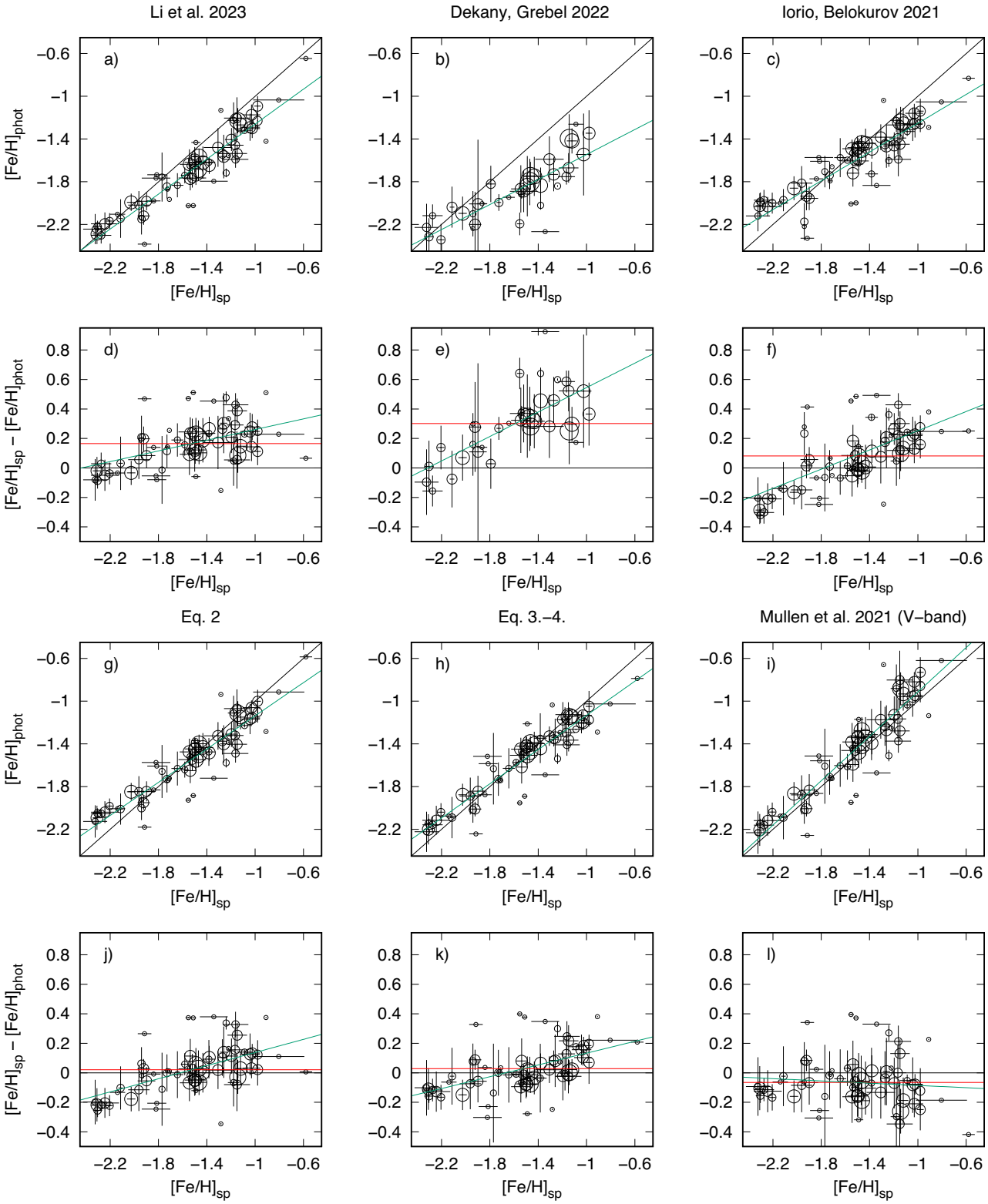

Figure 9. Comparison of the clusters mean $[Fe/H]_{phot}$ values derived from the Gaia photometric data using equation 1 of Li et al. (2023), the [Fe/H] values published by Dékány & Grebel (2022), calculated according to equation 3 of Iorio & Belokurov (2021), and equations (2), (3), and (4) of this paper with their spectroscopic metallicities ($[Fe/H]_{sp}$) are shown in the panels of (a), (b), (c), (g), (h), respectively, while panel (i) plots the *V* band $[Fe/H]_{phot}$ results using equations 6 and 9 of Mullen et al. (2021) after transforming our *G* band φ_{31} values to *V* band. The circles size is scaled according to the number of the LCs used in the cluster, the horizontal and vertical error-bars indicate the scatter of the $[Fe/H]_{sp}$ and the $[Fe/H]_{phot}$ values. The (d), (e), (f), (j), (k), (l) panels document the differences between the $[Fe/H]_{sp}$ and the mean $[Fe/H]_{phot}$ values. The black lines show the identity or the zero functions, while the green and red lines correspond to linear or constant fits to the data. Results obtained using the stars of Sample A are plotted in this figure, with the exception of panes (b) and (e).

Oo-type I and II variables separately are shown in panels (g) and (h). Panels (d), (e), (f), (j), and (k) show the differences between the mean $[Fe/H]_{phot}$ and $[Fe/H]_{sp}$ cluster values of the respective data. The panels, (i) and (l), document the results using equation 6 of Mullen et al. (2021) after applying the transformation between the V and G band φ_{31} parameters according to the formula given in Clementini et al. (2016). The black lines show the identity or the zero functions, while the green and red lines correspond to linear and constant fits to the data, respectively.

Notwithstanding that the calibrating samples of both the LC parameters and the [Fe/H] values, which the different Gaia-band photometric metallicity determinations are based on, are different, the estimated mean cluster metallicities show consistent results, with the exception of the overall zero-point differences between the results. Each $[Fe/H]_{phot}$ estimate tends to over- and to under-estimate the [Fe/H] towards the metal-poor and metal-rich ends, respectively, when the mean zero-offsets are taken into account [see (d), (e), (f), (j), and (k) panels in Fig. 9]. This systematic bias of the results is the smallest in panels (d) and (k) i.e. when the three parameter formula of Li et al. (2023), and when different formulae for the different Oo-type variables [equations (3) and (4)] are applied. However, none of the G band methods can eliminate this trend of the residuals completely. On the other hand, the V band formula (Mullen et al. 2021) does not show any systematic bias of the results, but an increased scatter in the $[-1.0: -1.6]$ [Fe/H] interval is evident in this case. This latter may be the consequence of that simple linear/constant transformations between the phase-parameters in different photometric bands might possess additional uncertainties.

Except an overall shift, the results obtained by using equation 1 of Li et al. (2023) [panels (a), (d)] and equations (2), (3), and (4) [panels (g), (j), (h), and (k)] seems to be the most compatible with each other, although the formulae are quite different. Li et al. (2023) established a three parameter (p, φ_{31}, R_{21}) formula, while we could not improve the fitting accuracy by using any additional parameter.

The calibration of the formula published by Li et al. (2023) relies on the [Fe/H] values of the Liu et al. (2020) catalogue and the LC parameters given in the Gaia DR3 catalogue. Their calibrating sample consists of about 2000 stars with metallicity distribution similar to the distribution in our GC sample. The [Fe/H] of the overwhelming majority of their stars fall in the -1 to -2 metallicity range (see fig. 2 in Li et al. 2023). The Liu et al. (2020) catalogue values are calibrated to field and GC data adopting $\log\epsilon Fe_{\odot} = 7.50$ and $\log\epsilon Fe_{\odot} = 7.54$ solar abundances, respectively. As a consequence of our choice of the $\log\epsilon Fe_{\odot} = 7.50$ solar reference value there should be a $\sim$0.02 dex offset between the results of the formulae published by Li et al. (2023) and derived in Section 3. However, as it can be seen in Fig. 9 there is about 0.17 dex difference between the results, which cannot be explained by the difference of the solar reference values. As the metallicity distribution of the two calibrations are similar, this also cannot explain the differences of the means.

The [Fe/H] data obtained by Dékány & Grebel (2022) [panels (b) and (e) in Fig. 9] show an even larger offset, the average $[Fe/H]_{sp} - [Fe/H]_{phot}$ difference is 0.30 dex. This data is based on the photometric metallicities derived from an I band metallicity formula (Dékány et al. 2021). The spectroscopic [Fe/H] data behind the Dékány & Grebel (2022) results were homogenized to match the metallicities published by Crestani et al. (2021), and this work accepted $\log\epsilon Fe_{\odot} = 7.50$ solar value. Consequently, the difference in the solar reference values does not explain the offset between the results. Besides the large offset, the scatter and the amplitude of the systematic of the differences of the mean $[Fe/H]_{sp} - [Fe/H]_{phot}$ cluster metallicities [see panel (e)] for their [Fe/H] values is also larger than for the other [Fe/H] estimates. This might be because of the poorer quality of the LCs of the Gaia DR2 than in the DR3 archive and also because that the I band photometric metallicities they used for calibration are, most probably, already affected by some systematic bias. Equation 3 of Iorio & Belokurov (2021) involves only the period and φ_{31} in the fitting process similarly to the relations presented here and they use the DR2 LCs. Their results, which are calibrated to the [Fe/H] values of Layden (1994) is the closest in zero-point to our accepted scale, however, as these [Fe/H] values are calibrated to an inhomogeneous sample of spectroscopic results and on the Zinn & West metallicities of globular clusters (Zinn & West 1984), it cannot be directly established, how much part of this offset comes from the differences in the reference solar values. Despite the same parameters involved, and the similarity of the results, their coefficients differ significantly from the coefficients of equation (2). The scatter of the results and the range of the residual differences of the Iorio & Belokurov (2021) formula is only marginally larger than for the results of Li et al. (2023) and of the formulae given in Section 3.

6 SUMMARY AND CONCLUSIONS

New $[Fe/H]_{phot}$ formulae of RRab stars in the Gaia G band are derived utilizing globular cluster data exclusively. The calibration of the formulae relies on a new compilation of the spectroscopic [Fe/H] values of the clusters involved in the study. The clusters [Fe/H] values are unified, adopting $\log\epsilon Fe_{\odot} = 7.50$ as the solar reference value.

Similarly to many previous studies the period and the ϕ_{31} epoch-independent phase difference are the LC parameters that yield the best estimate of the [Fe/H]. The fitting accuracy could not be improved using non-linear or multiparameter formulae. Based on the detection that the linear V and I band [Fe/H] formulae yield systematically different results for Oo-type I and II variables (Jurcsik et al. 2021), formulae have also been derived for the two Oo types separately. The fitting accuracy of the results could not be increased significantly this way, but the systematic $\sim$0.2 dex bias at the low-metallicity end is reduced to $\sim$0.1 dex. This procedure has also revealed that the scatter of the results for Oo-type II stars is larger than for the compete sample, additionally, most of the variables omitted from the fits because of their anomalous $[Fe/H]_{phot}$ values belong to this class of variables.

It seems that the Oo-type II sample of RRab stars does not follow any photometric metallicity relation strictly. Although no general census on the the explanation of the Oosterhoff dichotomy has been reached yet (see e.g. Catelan 2009), horizontal-branch evolution and morphology are some of the main issues that influence the structure of the period-amplitude diagram. In an early study of synthetic horizontal-branch evolution models, Lee, Demarque & Zinn (1990) showed that, in part, 'evolution away from the zero age horizontal branch (ZAHB) will play a role in the Oosterhoff group II clusters by increasing the mean luminosity and lowering the mean mass of the stars in the instability strip over the values predicted by ZAHB models'. The examination of the period-amplitude relation by Clement & Shelton (1999) supported the hypothesis that most RRL variables in Oo-type I clusters are ZAHB objects while those in the Oo-type II clusters are more evolved. Bono et al. (2020) concluded that 'evolutionary effects take account of the vertical structure (dispersion in amplitude) of the Bailey diagram based on radial velocity amplitudes'. As we separated Oo-type I and II stars based on their location on the period-amplitude plane, it is plausible

to suppose that variables with significantly different amplitudes at fixed period values are in different evolutionary stages.

Therefore, we surmise that Oo-type II stars, most probably, have already evolved off the ZAHB, and their physical structures may show larger diversity than the structures of RRLs close to the ZAHB evolutionary stage. This might be the reason for the decreased efficiency of the photometric metallicity formula for Oo-type II variables than for Oo-type I stars.

The inherent accuracy of any simple photometric [Fe/H] formula may be set by the heterogeneity of the variables. We think that the more homologous the variables in a sample, the more accurate $[Fe/H]_{phot}$ formula is valid for that sample.

The comparison of our [Fe/H] estimates with published Gaia *G* band photometric metallicities of RRab stars has also led to the conclusion that none of the photometric metallicity formula valid in this band yields similarly accurate [Fe/H] values all along the possible metallicity range and for variables evolved off the ZAHB. Involving extra parameters in the fits or the application of a complex deep learning method (Dékány & Grebel 2022) does not seem to improve the results (see Fig. 9) substantially.

We have detected significant differences between the zero points of the different photometric metallicity calibrations, which cannot be attributed to the differences between the accepted solar reference [Fe/H] values. This problem warns, that accurate reference [Fe/H] values on a homogeneous scale are highly needed. The compilation of the GC [Fe/H] data given in Section 2.2 aims to help in this problem in part.

ACKNOWLEDGEMENTS

This work has made use of data from the European Space Agency (ESA) mission *Gaia* (https://www.cosmos.esa.int/gaia), processed by the *Gaia* Data Processing and Analysis Consortium (DPAC, https://www.cosmos.esa.int/web/gaia/dpac/consortium). Funding for the DPAC has been provided by national institutions, in particular the institutions participating in the *Gaia* Multilateral Agreement. This research has been supported by the Hungarian National Research, Development, and Innovation Office (NKFIH) grants NN-129075 and K-129249. The research leading to these results has received funding from the European Research Council (ERC) under the European Union's Horizon 2020 research and innovation programme (grant agreement No. 695099).

DATA AVAILABILITY

The paper utilizes data of the Gaia DR3 archive, and published [Fe/H] values of globular clusters, all of which are publicly available.

REFERENCES

Arellano Ferro A., 2022, *Rev. Mex. Astron. Astrofis.*, **58**, 257
Asplund M., Grevesse N., Sauval A. J., Scott P., 2009, *ARA&A*, **47**, 481
Baeza I. et al., 2022, *A&A*, **662**, A47
Bailin J., 2019, *ApJS*, **245**, 5
Barbuy B. et al., 2018, *A&A*, **619**, A178
Bellinger E. P., Kanbur S. M., Bhardwaj A., Marconi M., 2020, *MNRAS*, **491**, 4752
Boberg O. M., Friel E. D., Vesperini E., 2016, *ApJ*, **824**, 5
Bono G. et al., 2019, *ApJ*, **870**, 115
Bono G. et al., 2020, *ApJ*, **896**, L15
Bradford J. D. et al., 2011, *ApJ*, **743**, 167
Bragaglia A., Carretta E., Sollima A., Donati P., D'Orazi V., Gratton R. G., Lucatello S., Sneden C., 2015, *A&A*, **583**, A69
Bragaglia A., Carretta E., D'Orazi V., Sollima A., Donati P., Gratton R. G., Lucatello S., 2017, *A&A*, **607**, A44
Cabrera-Ziri I., Lardo C., Mucciarelli A., 2019, *MNRAS*, **485**, 4128
Carlos M. et al., 2023, *MNRAS*, **519**, 1695
Carretta E., 2015, *ApJ*, **810**, 148
Carretta E., Bragaglia A., Gratton R., D'Orazi V., Lucatello S., 2009, *A&A*, **508**, 695
Carretta E. et al., 2010, *ApJ*, **714**, L7
Carretta E., Lucatello S., Gratton R. G., Bragaglia A., D'Orazi V., 2011, *A&A*, **533**, A69
Carretta E. et al., 2013, *A&A*, **557**, A138
Carretta E., Bragaglia A., Gratton R. G., D'Orazi V., Lucatello S., Sollima A., 2014a, *A&A*, **561**, A87
Carretta E. et al., 2014b, *A&A*, **564**, A60
Carretta E. et al., 2015, *A&A*, **578**, A116
Catelan M., 2009, *Ap&SS*, **320**, 261
Chun S.-H., Lee J.-J., Lim D., 2020, *ApJ*, **900**, 146
Clement C. M., Shelton I., 1999, *ApJ*, **515**, L85
Clement C. M. et al., 2001, *AJ*, **122**, 2587
Clementini G. et al., 2016, *A&A*, **595**, A133
Clementini G. et al., 2022, *A&A*, **674**, A18
Cohen J. G., 2011, *ApJ*, **740**, L38
Cohen J. G., Huang W., Kirby E. N., 2011, *ApJ*, **740**, 60
Crestani J., Alves-Brito A., Bono G., Puls A. A., Alonso-García J., 2019, *MNRAS*, **487**, 5463
Crestani J. et al., 2021, *ApJ*, **908**, 20
D'Orazi V., Campbell S. W., Lugaro M., Lattanzio J. C., Pignatari M., Carretta E., 2013, *MNRAS*, **433**, 366
Dékány I., Grebel E. K., Pojmański G., 2021, *ApJ*, **920**, 33
Dékány I., Grebel E. K., 2022, *ApJS*, **261**, 33
Deras D., Cadelano M., Ferraro F. R., Lanzoni B., Pallanca C., 2023, *ApJ*, **942**, 104
Dias B. et al., 2015, *A&A*, **573**, A13
Dias B., Saviane I., Barbuy B., Held E. V., Da Costa G., Ortolani S., Gullieuszik M., 2016a, *The Messenger*, **165**, 19
Dias B., Barbuy B., Saviane I., Held E. V., Da Costa G. S., Ortolani S., Gullieuszik M., Vásquez S., 2016b, *A&A*, **590**, A9
Ernandes H., Barbuy B., Alves-Brito A., Friaça A., Siqueira-Mello C., Allen D. M., 2018, *A&A*, **616**, A18
Fabrizio M. et al., 2021, *ApJ*, **919**, 118
Fernández-Trincado J. G. et al., 2021, *A&A*, **648**, A70
Frelijj H., Villanova S., Muñoz C., Fernández-Trincado J. G., 2021, *MNRAS*, **503**, 867
Gaia Collaboration, 2016, *A&A*, **595**, A1
Gaia Collaboration, 2022, *A&A*, **674**, A1
Geisler D. et al., 2021, *A&A*, **652**, A157
Geisler D. et al., 2023, *A&A*, **669**, A115
Givens R. A., Pilachowski C. A., 2016, *PASP*, 128, 124203
Gratton R. G., Carretta E., Claudi R., Lucatello S., Barbieri M., 2003, *A&A*, **404**, 187
Gratton R. G., Villanova S., Lucatello S., Sollima A., Geisler D., Carretta E., Cassisi S., Bragaglia A., 2012, *A&A*, **544**, A12
Gratton R. G. et al., 2013, *A&A*, **549**, A41
Gratton R. G. et al., 2015, *A&A*, **573**, A92
Grevesse N., Asplund M., Sauval A. J., 2007, *Space Sci. Rev.*, **130**, 105
Hanke M., Koch A., Hansen C. J., McWilliam A., 2017, *A&A*, **599**, A97
Harris W. E., 1996, *AJ*, **112**, 1487
Harris W. E., 2010, preprint (arXiv:1012.3224)
Horta D. et al., 2020, *MNRAS*, **493**, 3363
Iorio G., Belokurov V., 2021, *MNRAS*, **502**, 5686
Johnson C. I. et al., 2015, *AJ*, **149**, 71
Johnson C. I., Caldwell N., Rich R. M., Pilachowski C. A., Hsyu T., 2016, *AJ*, **152**, 21
Johnson C. I., Caldwell N., Rich R. M., Walker M. G., 2017a, *AJ*, **154**, 155
Johnson C. I., Caldwell N., Rich R. M., Mateo M., Bailey John I.I., Clarkson W. I., Olszewski E. W., Walker M. G., 2017b, *ApJ*, **836**, 168
Johnson C. I., Caldwell N., Rich R. M., Mateo M., Bailey John I.I., Olszewski E. W., Walker M. G., 2017c, *ApJ*, **842**, 24

Johnson C. I., Rich R. M., Caldwell N., Mateo M., Bailey John I.I., Olszewski E. W., Walker M. G., 2018, *AJ*, **155**, 71
Johnson C. I., Caldwell N., Michael Rich R., Mateo M., Bailey J. I., 2019, *MNRAS*, **485**, 4311
Jurcsik J., Kovács G., 1996, *A&A*, **312**, 111
Jurcsik J., Hajdu G., Juhász Á., 2021, *MNRAS*, **505**, 2468
Kacharov N., Koch A., McWilliam A., 2013, *A&A*, **554**, A81
Koch A., Côté P., 2019, *A&A*, **632**, A55
Koch A., McWilliam A., 2014, *A&A*, **565**, A23
Koch-Hansen A. J., Hansen C. J., McWilliam A., 2021, *A&A*, **653**, A2
Kolláth Z., 1990, *Konkoly Observatory Occasional Technical Notes*, **1**, 1
Kovalev M., Bergemann M., Ting Y.-S., Rix H.-W., 2019, *A&A*, **628**, A54
Lai D. K., Smith G. H., Bolte M., Johnson J. A., Lucatello S., Kraft R. P., Sneden C., 2011, *AJ*, **141**, 62
Lamb M. P., Venn K. A., Shetrone M. D., Sakari C. M., Pritzl B. J., 2015, *MNRAS*, **448**, 42
Lapenna E., Mucciarelli A., Ferraro F. R., Origlia L., Lanzoni B., Massari D., Dalessandro E., 2015, *ApJ*, **813**, 97
Lardo C., Mucciarelli A., Bastian N., 2016, *MNRAS*, **457**, 51
Layden A. C., 1994, *AJ*, **108**, 1016
Lee Y.-W., Demarque P., Zinn R., 1990, *ApJ*, **350**, 155
Li X.-Y., Huang Y., Liu G.-C., Beers T. C., Zhang H.-W., 2023, *ApJ*, **944**, 88
Liu G. C. et al., 2020, *ApJS*, **247**, 68
Lucertini F., Monaco L., Caffau E., Mucciarelli A., Villanova S., Bonifacio P., Sbordone L., 2022, *A&A*, **671**, A137
MacLean B. T., Campbell S. W., De Silva G. M., Lattanzio J., D'Orazi V., Simpson J. D., Momany Y., 2016, *MNRAS*, **460**, L69
MacLean B. T. et al., 2018, *MNRAS*, **481**, 373
Magurno D. et al., 2018, *ApJ*, **864**, 57
Magurno D. et al., 2019, *ApJ*, **881**, 104
Malavolta L., Sneden C., Piotto G., Milone A. P., Bedin L. R., Nascimbeni V., 2014, *AJ*, **147**, 25
Marconi M. et al., 2015, *ApJ*, **808**, 50
Marino A. F., Villanova S., Milone A. P., Piotto G., Lind K., Geisler D., Stetson P. B., 2011, *ApJ*, **730**, L16
Marino A. F. et al., 2014a, *MNRAS*, **437**, 1609
Marino A. F. et al., 2014b, *MNRAS*, **442**, 3044
Marino A. F. et al., 2017, *ApJ*, **843**, 66
Marino A. F. et al., 2018, *ApJ*, **859**, 81
Marino A. F. et al., 2019, *MNRAS*, **487**, 3815
Marino A. F. et al., 2021, *ApJ*, **923**, 22
Massari D. et al., 2017, *MNRAS*, **468**, 1249
Masseron T. et al., 2019, *A&A*, **622**, A191
McKenzie M. et al., 2022, *MNRAS*, **516**, 3515
Mészáros S. et al., 2020, *MNRAS*, **492**, 1641
Milone A. P. et al., 2015, *MNRAS*, **447**, 927
Monaco L., Villanova S., Bonifacio P., Caffau E., Geisler D., Marconi G., Momany Y., Ludwig H. G., 2012, *A&A*, **539**, A157
Monty S., Yong D., Marino A. F., Karakas A. I., McKenzie M., Grundahl F., Mura-Guzmán A., 2023, *MNRAS*, **518**, 965
Muñoz C., Geisler D., Villanova S., 2013, *MNRAS*, **433**, 2006
Muñoz C., Geisler D., Villanova S., Sarajedini A., Frelijj H., Vargas C., Monaco L., O'Connell J., 2021, *MNRAS*, **506**, 4676
Mucciarelli A., Team Cosmic-Lab, 2016, *Mem. Soc. Astron. Italiana*, **87**, 658
Mucciarelli A., Salaris M., Lovisi L., Ferraro F. R., Lanzoni B., Lucatello S., Gratton R. G., 2011, *MNRAS*, **412**, 81
Mucciarelli A., Bellazzini M., Ibata R., Merle T., Chapman S. C., Dalessandro E., Sollima A., 2012, *MNRAS*, **426**, 2889
Mucciarelli A., Lapenna E., Massari D., Ferraro F. R., Lanzoni B., 2015, *ApJ*, **801**, 69
Mucciarelli A. et al., 2016, *ApJ*, **824**, 73
Mucciarelli A., Lapenna E., Ferraro F. R., Lanzoni B., 2018, *ApJ*, **859**, 75
Mullen J. P. et al., 2021, *ApJ*, **912**, 144
Mullen J. P. et al., 2023, *ApJ*, **945**, 83
Nemec J. M., Cohen J. G., Ripepi V., Derekas A., Moskalik P., Sesar B., Chadid M., Bruntt H., 2013, *ApJ*, **773**, 181
O'Malley E. M., Chaboyer B., 2018, *ApJ*, **856**, 130
Pancino E. et al., 2017, *A&A*, **601**, A112
Pritzl B., Smith H. A., Catelan M., Sweigart A. V., 2000, *ApJ*, **530**, L41
Pritzl B. J., Smith H. A., Catelan M., Sweigart A. V., 2002, *AJ*, **124**, 949
Puls A. A., Alves-Brito A., Campos F., Dias B., Barbuy B., 2018, *MNRAS*, **476**, 690
Roederer I. U., Marino A. F., Sneden C., 2011, *ApJ*, **742**, 37
Roederer I. U., Sneden C., 2011, *AJ*, **142**, 22
Roederer I. U., Thompson I. B., 2015, *MNRAS*, **449**, 3889
Roederer I. U., Mateo M., Bailey J. I., Spencer M., Crane J. D., Shectman S. A., 2016, *MNRAS*, **455**, 2417
Rojas-Arriagada A., Zoccali M., Vásquez S., Ripepi V., Musella I., Marconi M., Grado A., Limatola L., 2016, *A&A*, **587**, A95
Saviane I., Da Costa G. S., Held E. V., Sommariva V., Gullieuszik M., Barbuy B., Ortolani S., 2012, *A&A*, **540**, A27
Sbordone L. et al., 2015, *A&A*, **579**, A104
Schaeuble M., Preston G., Sneden C., Thompson I. B., Shectman S. A., Burley G. S., 2015, *AJ*, **149**, 204
Simmerer J., Ivans I. I., Filler D., Francois P., Charbonnel C., Monier R., James G., 2013, *ApJ*, **764**, L7
Smolec R., 2005, *AcA*, **55**, 59
Sobeck J. S. et al., 2011, *AJ*, **141**, 175
Sollima A., Borissova J., Catelan M., Smith H. A., Minniti D., Cacciari C., Ferraro F. R., 2006, *ApJ*, **640**, L43
Souza S. O. et al., 2023, *A&A* **671** A45
Spite M., Spite F., Gallagher A. J., Monaco L., Bonifacio P., Caffau E., Villanova S., 2016, *A&A*, **594**, A79
Tautvaišienė G. et al., 2022, *A&A*, **658**, A80
Valenti E., Origlia L., Rich R. M., 2011, *MNRAS*, **414**, 2690
Vargas C., Villanova S., Geisler D., Muñoz C., Monaco L., O'Connell J., Sarajedini A., 2022, *MNRAS*, **515**, 1903
Vasiliev E., Baumgardt H., 2021, *MNRAS*, **505**, 5978
Vásquez S. et al., 2018, *A&A*, **619**, A13
Villanova S., Geisler D., 2011, *A&A*, **535**, A31
Villanova S., Geisler D., Piotto G., Gratton R. G., 2012, *ApJ*, **748**, 62
Villanova S., Geisler D., Carraro G., Moni Bidin C., Muñoz C., 2013, *ApJ*, **778**, 186
Villanova S., Monaco L., Moni Bidin C., Assmann P., 2016, *MNRAS*, **460**, 2351
Villanova S., Moni Bidin C., Mauro F., Munoz C., Monaco L., 2017, *MNRAS*, **464**, 2730
Wang Y., Primas F., Charbonnel C., Van der Swaelmen M., Bono G., Chantereau W., Zhao G., 2016, *A&A*, **592**, A66
Wang Y., Primas F., Charbonnel C., Van der Swaelmen M., Bono G., Chantereau W., Zhao G., 2017, *A&A*, **607**, A135
Worley C. C., Hill V., Sobeck J., Carretta E., 2013, *A&A*, **553**, A47
Yong D. et al., 2014a, *MNRAS*, **439**, 2638
Yong D. et al., 2014b, *MNRAS*, **441**, 3396
Yong D., Grundahl F., Norris J. E., 2015, *MNRAS*, **446**, 3319
Zinn R., West M. J., 1984, *ApJS*, **55**, 45

This paper has been typeset from a TEX/LATEX file prepared by the author.